Polymer 231 (2021) 124110

Contents lists available at ScienceDirect

Polymer

journal homepage: www.elsevier.com/locate/polymer

Thiol–acrylate based vitrimers: From their structure–property relationship to the additive manufacturing of self-healable soft active devices

Usman Shaukat, Elisabeth Rossegger, Sandra Schlögl *

Polymer Competence Center Leoben GmbH, Roseggerstrasse 12, 8700, Leoben, Austria

ARTICLE INFO

Keywords:
Vitrimers
Self-healing
Thermo-activated transesterification
Additive manufacturing

ABSTRACT

Thiol-acrylate based vitrimers combine the advantages of dynamic covalent bonds with the salient features of "click" chemistry including low shrinkage stress and homogenous network properties. The poor storage stability of thiol-acrylate formulations can be overcome by adding an acidic organic phosphate as stabilizer, which at the same time acts as an efficient catalyst to induce transesterifications at elevated temperature. At a sufficiently high rate, the dynamic bond exchange reactions lead to topological rearrangements and a related macroscopic reflow of the photopolymer network. This paves the way towards dynamic photopolymers, which are thermally mendable, malleable, reprocessable and have shape memory properties. In this work, a library of thiol-acrylate monomers for the preparation of digital light processable (DLP) vitrimers is systematically studied. In particular, thiol crosslinkers with varying functionality and number of ester moieties are employed and combined with selected mono- and bi-functional acrylates bearing free –OH groups. In addition, vitrimer networks with higher crosslink density are prepared by adding tri- and tetra-functional acrylates to the formulations. In a comprehensive way, the effect of crosslinking density, monomer structure, network architecture and thermal annealing on cure kinetics, mechanical, thermal and vitrimeric properties of the dynamic photopolymers are studied. The results reveal that by appropriate network design, thermal and mechanical properties of the networks can be controlled over a wide range. In particular, a high mobility of the polymer chains together with a high number of –OH and ester groups is beneficial for inducing fast exchange reactions. The proposed thiol-acrylate based vitrimers show a great potential for the personalized fabrication of soft active devices and their applicability in DLP 3D-printed soft actuators with adequate stretchability and thermal mendability is highlighted.

1. Introduction

Thermosets and rubbers are crosslinked networks formed by connecting polymer chains through covalent bonding, which makes them mechanically strong and resistant towards solvents and environmental conditions. The crosslinking is further vital to adjust thermal and mechanical properties of polymeric materials [1–4]. But these covalent crosslinks also render the polymer networks infusible and thus, strictly hinder their reprocessability.

Associative covalent adaptable networks (CANs) have the potential to overcome these challenges and have gained increased attention in recent years [5]. Associative CANs are dynamic polymer networks which are able to undergo thermo-activated bond exchange reactions. At lower temperatures, these bond exchange reactions occur at a slow rate and the materials behave like permanent networks. With increasing temperature, the dynamic bond exchanges become significantly faster and lead to topological rearrangements of the network. The temperature, below which vitrimeric networks act as permanently crosslinked networks, is termed topology freezing temperature (T_v) [6,7]. In contrast to dissociative CANs (e.g. relying on Diels Alder chemistry), associative CANs maintain their overall network connectivity during bond exchange reactions. Consequently, the viscosity of vitrimers does not exhibit a sharp drop with increasing temperature like thermoplastic polymers, but follows an Arrhenius behavior [8,9].

Due to the unique properties of associative CANs, various dynamic covalent chemistries have been reported over the past years including olefin metathesis [10], boron ester exchanges [11–13], transamination of vinylogous urethanes [14–17], disulfide exchange [18–21], transesterification [9,22–26], transcarbamoylation [27] and vinylogous urethane transamination [14,28]. In particular, associative CANs based on transesterifications are one of the most popular dynamic networks [9, 29–34], due to the ease of manufacturing, excellent properties and also

* Corresponding author.
E-mail address: sandra.schloegl@pccl.at (S. Schlögl).

https://doi.org/10.1016/j.polymer.2021.124110
Received 9 May 2021; Received in revised form 13 August 2021; Accepted 17 August 2021
Available online 22 August 2021

due to the large variety of readily available chemicals with suitable functionalities. They were firstly introduced by Leibler and co-workers, who termed them vitrimers according to their temperature-dependent viscosity, which is comparable to strong glass forming liquids [34,35]. Along with classical epoxy-based thermosets [36] and elastomers [37–39], dynamic bonds based on thermo-activated transesterifications have also been applied recently in 3D-printable materials. This enables the additive manufacturing of devices with high resolution, complex geometries and additional functionalities such as mendability and recyclability [39–42]. In addition, their shape memory characteristics can provide step-changes in the fabrication of functional and personalized devices for application areas such as medicine [43], electronics [44,45] and soft-robotics [46,47].

Among the various printing techniques, digital light processing (DLP) 3D-printing offers significant advantages such as high resolution, good surface quality of the printed parts and adequate building speed. During DLP 3D-printing, a liquid resin is photochemically cured layer-by-layer by spatially controlled light exposure in a vat (Fig. 1a) [48,49]. Recently, we successfully DLP 3D-printed acrylate and thiol-acrylate based vitrimers by replacing well established transesterification catalysts such as $Zn(OAc)_2$ or Brønsted bases with organic phosphates. In particular, we were able to obtain photo-reactive 3D-printable resin formulations, which were characterized by fast cure rates and a high storage stability [39,50,51].

Advancing from proof of concept studies, the current work details structure-property relationships of thiol-acrylate based vitrimers to obtain soft active devices with adjustable (thermo)mechanical performance and fast relaxation kinetics. A further focus is placed on the cure kinetics of the formulations, as the processing of the vitrimeric photopolymers via DLP represents a key factor for the fabrication of personalized soft active devices.

For the systematic study, we chose acrylates as “ene” components and thiol crosslinkers with varying functionality and number of –OH and ester moieties (Fig. 2), which are crucial for the transesterification and corresponding network relaxation (Fig. 1b). By going from the molecular structure of the monomers over the relaxation of the vitrimer networks to the final mechanical properties, a correlation of network architecture and related thermo-mechanical performance of thiol-acrylate vitrimers is obtained. In addition, the applicability of the systems for the additive manufacturing of healable soft active devices is highlighted by the DLP 3D-printing of spring elements undergoing thermally induced actuations and which are mendable at elevated temperature.

2. Experimental

2.1. Materials and chemicals

2-Hydroxy-3-phenoxy propyl acrylate (HP1A), glycerol 1,3-diglycerolate diacrylate (DG2A), 1,6 hexane dithiol (HXDT), trimethylolpropane triacrylate (PT3A), pentaerythritol tetraacrylate (PT4A), ethylene glycol bis-mercaptoacetate (EGMA), phenylbis(2,4,6-trimethylbenzoyl) phosphine oxide and dichloromethane were supplied by Sigma-Aldrich and used as received. Ethylene glycol bis(3-mercaptopropionate) (EGMP), polycaprolactone tetra-mercaptopropionate (PCLMT), pentaerythritol tetrakis(3-mercapto-propionate) (PTTMP), dipentaerythritol hexakis(3-mercaptopropionate) (DPTHMP), were kindly provided by Bruno Bock Chemische Fabrik (Germany). Miramer A99 was obtained from Miwon Specialty Chemicals (Korea). The chemical structures of the components are provided in Fig. 2.

2.2. Sample preparation

HP1A (50 mol%), DG2A (25 mol%), along with 25 mol% of one of the thiols (Fig. 2) was mixed on a magnetic stirrer at room temperature for 1 h. For preparing formulations with multi-functional acrylates, PT3A (50 mol%) and PT4A (50 mol%) were mixed with DG2A (25 mol%) and EGMA (25 mol%). Furthermore, 2 wt% phenylbis(2,4,6-trimethylbenzoyl) phosphine oxide as photo-initiator, 0.05 wt% Sudan II as photoabsorber and 10 wt% of Miramer A99 as transesterification catalyst were added and the formulations were mixed for 1 h on a magnetic stirrer at room temperature. The photoabsorber was added to facilitate high resolution printing and to prevent “over-curing” of the resin in the vat. All formulations were prepared in light-protected glass vials and the compositions are summarized in Table 1.

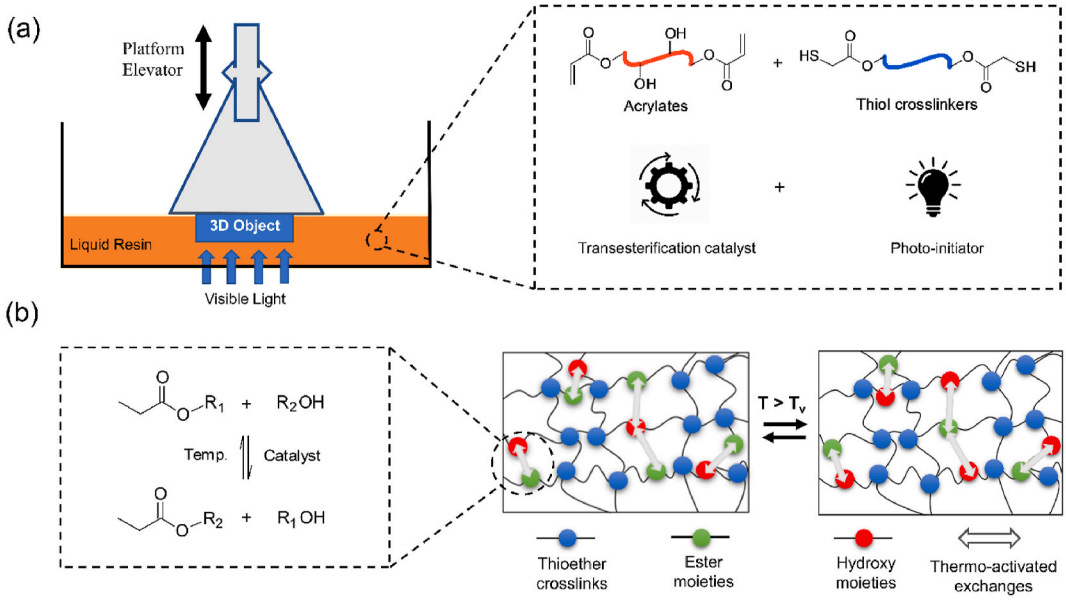

Fig. 1. (a) Schematic diagram of the digital light processing (DLP) 3D-printing technology and generalized structure of resin components applied for the additive manufacturing of thiol-acrylate vitrimers. (b) Schematic representation of the crosslinked network, which is capable of undergoing thermo-activated ($T > T_v$) and catalyzed transesterifications between hydroxyl and ester moieties present in thiol-acrylate vitrimers.

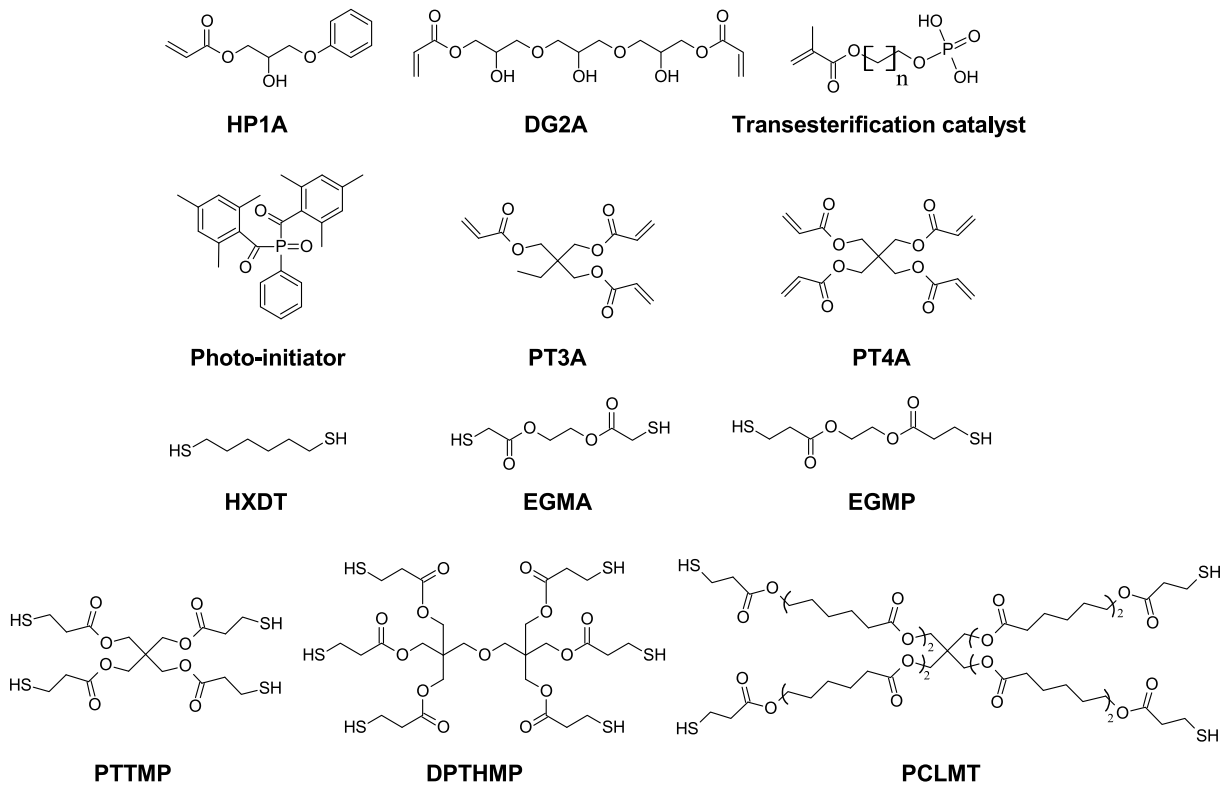

Fig. 2. Chemical structures of acrylate monomers, photo-initiator, transesterification catalyst and thiol crosslinkers used for the preparation of thiol-acrylate vitrimers.

Table 1
Composition of thiol-acrylate based vitrimers under investigation. All formulations contained 10 wt% Miramer A99, 2 wt% photo-initiator and 0.05 wt% Sudan II.

Formulation ID	Acrylate I (mol%)	Acrylate II (mol%)	Thiol (mol %)	Stoichiometric ratio (thiol:acrylate)
HXDT-HP1A	HP1A (50)	DG2A (25)	HXDT (25)	1:2
EGMA-HP1A	HP1A (50)	DG2A (25)	EGMA (25)	1:2
EGMP-HP1A	HP1A (50)	DG2A (25)	EGMP (25)	1:2
PCLMT-HP1A	HP1A (50)	DG2A (25)	PCLMT (25)	1:1
PTTMP-HP1A	HP1A (50)	DG2A (25)	PTTMP (25)	1:1
DPTHMP-HP1A	HP1A (50)	DG2A (25)	DPTHMP (25)	1.5:1
EGMA-PT3A	PT3A (50)	DG2A (25)	EGMA (25)	1:4
EGMA-PT4A	PT4A (50)	DG2A (25)	EGMA (25)	1:5

2.3. Digital light processing (DLP) 3D-Printing

DLP 3D-printing was carried out using an Anycubic Photon S printer (China) with a LED source of 405 nm. The exposure time of the bottom layer was 60 s whilst the other layers were exposed for 40 s based on the monomer conversions obtained from FTIR experiments. The layer thickness was 50 μm and both building speed and retracting speed amounted to 2 mm s^{-1}.

An Olympus BX 51 (Japan) optical microscope was used to take images of DLP 3D-printed test structures with a Color View IIIu digital camera (Soft Imaging System, Germany).

2.4. Characterization of network properties and reaction kinetics

FTIR spectra were taken to study the reaction progress versus the exposure time using a Vertex 70 spectrometer (Bruker, USA). 16 scans were measured for each exposure time in transmission mode from 4000 to 700 cm^{-1} with a resolution of 4 cm^{-1}. The area of the absorption peaks was calculated by OPUS software. 1.2 μL of liquid resin was drop-cast between two CaF_2 slides. For studying the kinetics of the photo-curing reaction, a LED lamp (zgood® wireless) with a power density of 3.3 mW cm^{-2} (λ = 420–450 nm) was used as a light source. The illumination and subsequent curing were performed until there was no change in the absorption peaks of thiol and acrylate absorption bands observed. The conversions at corresponding exposure times were calculated from the normalized peak areas of the characteristic acrylate (1635 cm^{-1}) and thiol (2570 cm^{-1}) groups using OPUS software.

FT-IR spectra of cured and thermally annealed (180 °C for 4 h under air) samples were taken with an FT-IR spectrometer (Vertex 70, Bruker, USA) equipped with a reflection diamond attenuated total reflection (ATR) accessory (Platinum ATR). For sample preparation, discs with a diameter of 10 mm and a height of 0.4 mm were 3D printed. 16 scans were measured for each sample from 4000 to 400 cm^{-1}.

Stress relaxation measurements were performed at 180 °C on DLP 3D-printed circular shaped (d = 10 mm) samples with a rheometer (Anton Paar Physica MCR-501, Austria) in a parallel plate arrangement. All samples were equilibrated at a force of 20 N for 20 min before recording the stress relaxation. A strain of 3% was applied and the decreasing stress was monitored over time.

For the evaluation of tensile properties, rectangular shaped samples with 30 × 10 × 1.5 mm (l x w x h) were 3D-printed via DLP. A Zwick-Roell Z1.0 static materials testing equipment (Germany) was used to measure the tensile properties of the samples at 250 mm min^{-1} cross-head speed. For each cured network, at least 5 sample were measured and the arithmetic average was taken.

Differential scanning calorimetry (Perking Elmer DSC 4000, USA)

was employed to measure the glass transition temperature (T_g) of cured samples. A heating rate of 15 K min^{-1} was applied between −80 °C and 200 °C under nitrogen atmosphere. The T_g was determined by taking the midpoint of the heat capacity from the second heating run.

A modular compact rheometer (MCR 102 Anton Paar, Austria) with a CP60–0.5/TI cone (49.97 mm diameter and 1.982° opening angle) was used to determine the viscosity of the resin. 1 mL of the liquid resin was analyzed at 25 °C with a shear rate ranging between 0.1 and 300 s^{-1}.

The gel content was measured by immersing DLP 3D printed discs (d = 20 mm, h = 1 mm) in dichloromethane at 20 °C for 48 h. Subsequently, the samples were removed and excess solvent was dried from the surface by using tissue paper. The swollen samples were placed at 40 °C in an oven until constant weight. The gel content was estimated by m_{dr}/m_{ini}, where m_{ini} represents the weight of the initial sample and m_{dr} being the weight of the dried sample. For each cured network, 5 samples were measured and the arithmetic average was taken.

2.5. Self-healing and thermal actuation experiments

For self-healing experiments, rectangular bars (30 × 10 × 1.5 mm) with a center hole of 5 mm, a circular disc (5 × 1.5 mm) and a control sample (30 × 10 × 1.5 mm) having no damage sites were DLP 3D-printed with resin formulation EGMA-PT3A. To demonstrate the self-healing properties of the samples, the circular discs were placed inside the bars and exposed to a temperature of 180 °C for 4 h under air. After self-healing the stress-strain properties of the samples were analyzed by using tensile testing and compared with the defect-free control samples.

For thermal actuation experiments, a spring (50 × 15 mm) was DLP 3D-printed by using the resin formulation EGMA-PT3A. A weight of approximately two times higher than the weight of the spring was attached and the temperature was increased to 65 °C, which was above the network's glass transition temperature (43 °C) and thus, resulted in a softening of the spring. The spring was manually elongated to an elongation of 70%. Thermally induced actuations were monitored by subsequently cooling it down to 20 °C. Moreover, the spring was broken by elongating it manually to an elongation of 80%, and it was thermally healed by bringing the damaged sites together and thermally annealing the sample at 180 °C for 4 h under air.

3. Results and discussion

3.1. Influence of thiol crosslinker on cure kinetics and properties of thiol-acrylate vitrimers

For the first study, thiol-acrylate based vitrimers were prepared by using a series of bi-functional thiols with varying number of ester moieties whilst keeping the concentration and ratio of –OH functional acrylate monomers (HP1A and DG2A) constant. In particular, the aliphatic 1,6-hexane dithiol (HXDT) containing no ester moiety and two mercapto esters (ethylene glycol bis-mercaptoacetate, EGMA, and ethylene glycol bis-3-mercaptopropionate, EGMP) were chosen as thiol crosslinker. The cure kinetics of the formulations were monitored by following the depletion of the characteristic stretching band of the S-H bond at 2570 cm^{-1} and the C=C bond wagging band at 1635 cm^{-1} over the exposure time (FT-IR spectra prior to and after UV exposure are provided in Fig. S1 in supporting information).

In all three resin formulations, the acrylate monomers reached a higher final monomer conversion (95%–97%) compared to the thiols (48%–55%) (Fig. 3a). This is explained by the participation of the acrylates in both chain-growth (homo-polymerization) and step-growth

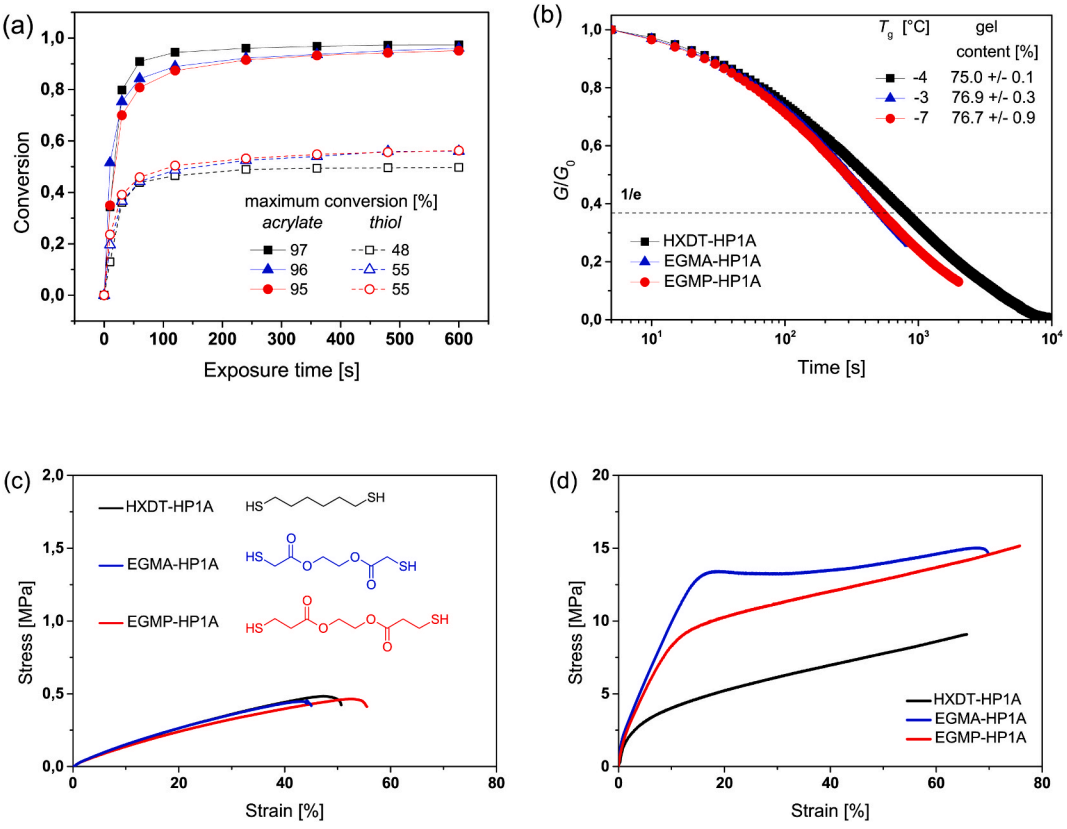

Fig. 3. (a) Cure kinetics and final monomer conversions of acrylate groups at 1635 cm^{-1} (full symbols) and thiol groups at 2570 cm^{-1} (open symbols) versus light exposure as obtained from FTIR experiments. As thiol crosslinker various bi-functional thiols have been applied: HXDT-HP1A (black squares), EGMA-HP1A (blue triangles), EGMP-HP1A (red circles). The lines are a guide for the eye. (b) Normalized stress relaxation curves of thiol-acrylate vitrimers measured at 180 °C. The table provides the glass transition temperature (T_g) and gel content of the respective networks. Stress-strain curves of thiol-acrylate vitrimers containing different bi-functional thiols (c) prior to and (d) after thermal annealing at 180 °C for 4 h.

polymerization reactions (thiol-ene addition reaction) as the photo-curing of thiol-acrylate resins follows a mixed-mode photo-polymerization mechanism [52]. The radical-mediated reaction is initiated by a homolytic cleavage of the Norrish type I photo-initiator. Radicals are formed, which abstract a hydrogen from a thiol group of the crosslinker, yielding a thiyl radical, which reacts with the C=C bond of the acrylate. A carbon centered radical is formed, which either abstracts a hydrogen from another thiol (step-growth mechanism) or undergoes an addition reaction to an acrylate group (chain-growth mechanism). Whilst chain growth polymerization leads to a fast increase in molecular weight, the step-growth polymerization favors the formation of low M_W species resulting in delayed gelation, lower shrinkage stress and a more homogenous network [53–57]. It should be noted that the thiols are not only able to undergo step-growth reactions but also act as chain transfer agents for the chain-growth polymerization of the acrylates and shift the gel point towards higher conversions. In a typical thiol-acrylate polymerization, the rate of acrylate homo-polymerization is 1.5 times higher than the rate of hydrogen abstraction from the thiol groups [58]. This is also reflected by the higher conversion of acrylates in the thiol-acrylate based vitrimers under investigation (Fig. 3a).

Comparing the cure kinetics of the different bi-functional thiols, it is obvious that HXDT as aliphatic thiol yielded a thiol-acrylate network (HXDT-HP1A), which was characterized by faster acrylate conversion and lower final thiol conversion compared to EGMA as mercapto acetic ester counterpart. This can be explained by the presence of the ester group in the structure of EGMA, which increases the reactivity of S-H bonds towards hydrogen abstraction [57].

In contrast, replacing the mercapto acetic ester (EGMA-HP1A) with the mercapto propionatic ester (EGMP-HP1A) did not significantly affect cure kinetics or final monomer conversion of the vitrimeric photopolymers.

It has to be considered, that in these three thiol-acrylate networks, crosslink points were predominately formed by the homo-polymerization of the bi-functional DG2A acrylate, whilst the bifunctional thiols acted as chain extenders and increased the molecular weight between two crosslinking points [59,60]. To determine the gel content of the networks, cured test specimen were immersed in dichloromethane for 48 h and the residual weight of the dried samples was taken. The three networks exhibited a gel content in the range of 75.0%–76.9%, which indicates a comparable crosslink density. The low gel content is related to an incomplete conversion of the monomers and particularly the thiol crosslinker, which were extracted from the networks during swelling. The residual thiols can act as lubricants and, together with the flexible thioether bonds formed by the thiol-ene reaction, imparted significant mobility into the networks, which had a glass transition temperature (T_g) well below room temperature (−4 °C to −7 °C). The related DSC curves are shown in Fig. S2 in supporting information.

For stress relaxation experiments, discs with a diameter of 10 mm were DLP 3D-printed and the impact of ester moieties on the exchange kinetics in the vitrimeric photopolymers under investigation was determined. The stress relaxation measurements were performed at 180 °C and the related curves are provided in Fig. 3b. For vitrimers, the characteristic time for stress relaxation is determined when the normalized modulus ($G_{(t)}/G_0$) reaches 37% of its initial value [39,51]. Regarding EGMA-HP1A and EGMP-HP1A, the time was comparable and amounted to 535 and 530 s, respectively. In contrast, HXDT-HP1A exhibited a slightly slower relaxation rate and required 765 s until ($G_{(t)}/G_0$) reached 37%. Since the crosslink density and T_g of the networks were in a similar range, the slower relaxation rate can be mainly related to the absence of ester groups in the molecular structure of HXDT. As the availability of –OH and ester groups is vital for bond exchange reactions, the exchange rate slows down with a lower concentration of functional groups, which was also observed in previous studies on thermally cured polyester based vitrimers [61].

Along with stress relaxation, the impact of ester moieties on the mechanical properties of the thiol-acrylate vitrimers were studied. Test specimens were DLP 3D-printed and tested uniaxially in tensile mode. Due to their low T_g, the networks were soft at room temperature and suffered from a low tensile strength, which was well below 0.5 MPa (Fig. 3c). The type of bi-functional thiol did not significantly affect the ultimate elongation, which varied between 45% and 55%. However, the picture completely changed when the networks were thermally annealed at 180 °C for 4 h prior to the tensile test. After annealing all three networks underwent a distinctive increase both in tensile strength and ultimate elongation (Fig. 3d). It is interesting to note that the increase was more pronounced for EGMA-HP1A and EGMP-HP1A (15 MPa) compared to HXDT-HP1A (9 MPa).

In general, the improvement of the toughness is attributed to thermo-activated rearrangements of the network and the reduction of shrinkage stress. Previous work revealed that the thermal treatment also facilitates hydrogen bonding, which further contributes to higher tensile properties [44,62]. Thus, the better performance of EGMA-HP1A and EGMP-HP1A can be explained by the presence of a higher number of ester groups, which accelerated the stress relaxation kinetics and enabled more hydrogen bonding with the –OH groups in the network.

To increase the number of crosslink points in the thiol-acrylate vitrimers, the bi-functional thiols were replaced by multi-functional derivatives. In particular, two tetra-functional thiols with varying spacer length (PTTMP and PCLMT) and ester functions, and a hexa-functional 3-mercaptopropionate (DPTHMP) were applied. HP1A and DG2A were chosen again as acrylate monomers and their concentration and ratio were kept constant in the formulations.

The FTIR studies revealed that both acrylate and thiol conversion decrease with rising functionality of the thiol (Fig. 4a), which is typical for radical-mediated thiol-ene reactions as the photopolymerization kinetics is governed by diffusion limitation of the reactive monomers. The increase in thiol functionality is related to a decrease in the conversion at which the gel point occurs and the polymerization rate slows down due to diffusional constraints [60]. Along with the functionality, diffusion limitations are also influenced by the structure of the thiol crosslinker. By using oligomers with relatively long and flexible spacers between the thiol functionalities, a higher conversion is obtained as the oligomeric radicals can still approach each other mainly via segmental diffusion or by propagation [63]. As the reaction proceeds and crosslink density increases, the movement of radical sites by propagation reactions becomes much faster compared to segmental diffusion. This effect can be observed when comparing the thiol conversion of PTTMP-HP1A and PCLMT-HP1A. PCLMT comprises polycaprolactone-based spacers between the thiol groups, which significantly increased the flexibility of the crosslinker and yielded higher thiol conversions (50%) compared to PTTMP as low molecular weight tetra-functional counterpart (43%). In terms of DPTHMP-HP1A, it has to be considered that this formulation contained an excess of thiol groups as the stoichiometric ratio between thiol and acrylate groups amounted to 1.5:1. Thus, the maximum conversion of the thiol groups is limited and along with diffusion limitations, the low final thiol conversion (42%) observed in DPTHMP-HP1A might be also associated with the excess of thiol groups in the formulation.

In terms of network mobility, the increase in the thiol functionality did not significantly affect the T_g of the networks, which only slightly decreased from −5 °C (EGMP-HP1A) to −8 °C (DPTHMP-HP1A). The DSC curves are provided in Fig. S2 in the supporting information. However, compared to EGMP-HP1A, the monomer conversion obtained with the multi-functional thiols resulted in lower gel contents, which ranged between 71.1 and 72.4%.

For EGMP, PTTMP and DPTHMP, which comprised a molar ratio of ester to thiol moieties of 1:1 (Fig. 2), the stress relaxation rates were comparable, with relaxation times of 490–515 s until ($G_{(t)}/G_0$) reaches 37% (Fig. 4b). In contrast, the PCLMT crosslinker had a molar ratio of ester to thiol moieties of 3:1, which yielded networks with a higher number of ester moieties since the stoichiometry of the acrylate and

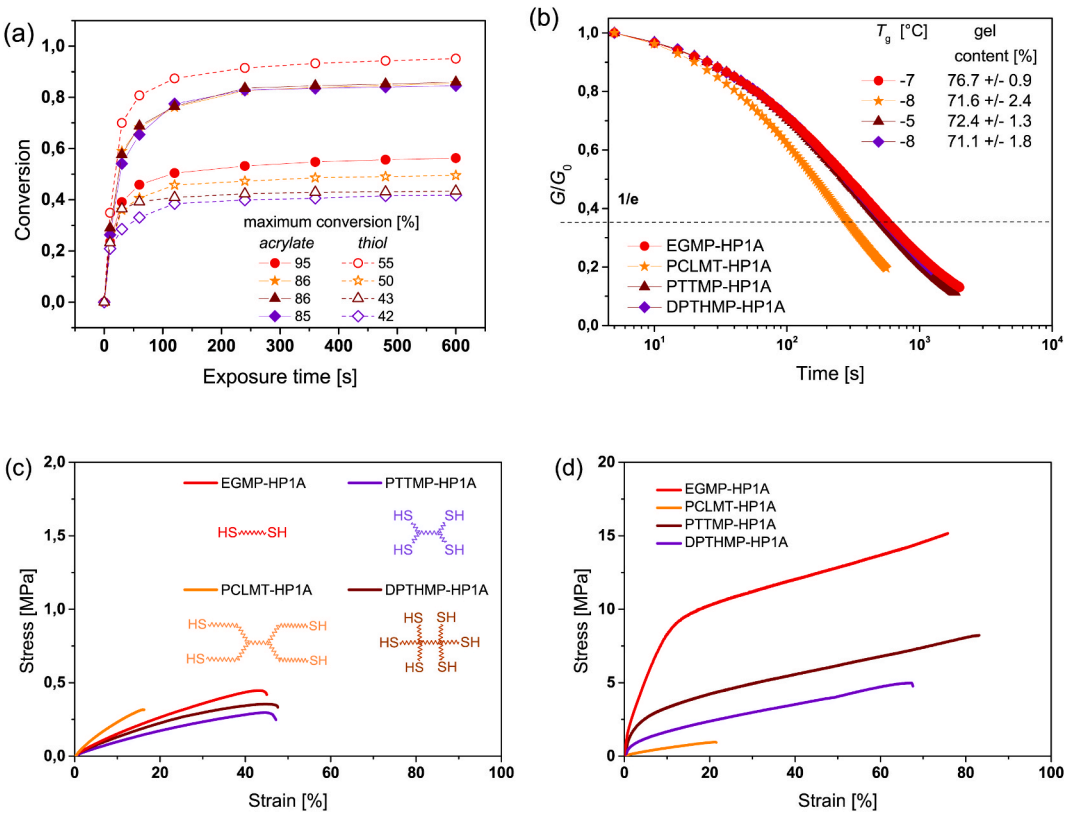

Fig. 4. (a) Cure kinetics and final monomer conversions of acrylate groups at 1635 cm^{-1} (full symbols) and thiol groups at 2570 cm^{-1} (open symbols) versus light exposure as obtained from FTIR experiments. As thiol crosslinker various multi-functional thiols have been applied: EGMP-HP1A (red circles), PCLMT-HP1A (orange stars), PTTMP-HP1A (brown triangles) and DPTHMP-HP1A (violet diamonds). The lines are a guide for the eye. (b) Normalized stress relaxation curves of thiol-acrylate vitrimers measured at 180 °C. The table provides the glass transition temperature (T_g) and gel content of the respective networks. Stress-strain curves of thiol-acrylate vitrimers containing different multi-functional thiols (c) prior to and (d) after thermal annealing at 180 °C for 4 h.

thiol groups were kept constant. The higher number of ester groups accelerated the relaxation kinetics and thus, the characteristic relaxation time of PCLMT-HP1A was nearly halved (270 s). The results are in good agreement with stress relaxation data on the above discussed thiol-acrylate networks containing bi-functional thiols (Fig. 3b) and confirm the important role of the number of ester functional groups in the exchange kinetics.

Increasing the functionality of the thiols did not improve the mechanical properties of the thiol-acrylate vitrimers at room temperature, which were having a strain at break between 18 and 55% and a tensile strength below 0.5 MPa (Fig. 4c). Although PCLMT-HP1A was characterized by a fast exchange rate, its poor tensile properties did not significantly increase by subsequent thermal annealing at 180 °C. In contrast, the toughness of PTTMP-HP1A and DPTHMP-HP1A networks improved by thermal annealing. However, it should be noted that the increase was less pronounced compared to EMGA-HP1A (Fig. 4d). This might be explained by the plasticization of the networks, which is expected to become a dominating mechanism at higher concentration of non-reacted thiols [64].

3.2. *Influence of acrylate monomers on cure kinetics and properties of thiol-acrylate vitrimers*

As the functionality of the thiols did not significantly affect the T_g and stress relaxation kinetics of the related thiol-acrylate vitrimers, the functionality of the acrylate monomers was varied in a further step. For this study, HP1A bearing one –OH group was replaced by the tri-functional PT3A and the tetra-functional PT4A, which did not contain any –OH moieties in their structure. Thus, along with the higher functionality, EGMA-PT3A and EGMA-PT4A networks were characterized by a lower number of free –OH groups. In these resin formulations, EGMA was used as thiol crosslinker and its content was kept constant (molar ratio of ester to thiol moieties in EGMA amounted to 1:1). The FTIR experiments showed that with rising functionality of the acrylate, involving a larger number of double bonds per monomer, the initial reaction rates of both acrylates and thiols increased (Fig. 5a). In particular, upon 10 s light exposure, the acrylate conversion of EGMA-HP1A amounted to 35% whilst it was well above 50% for EGMA-PT3A and EGMA-PT4A. However, in radically-induced chain-growth reactions a higher degree of functionality also leads to a more rapid onset of gelation and a higher crosslink density. The higher crosslink density of EGMA-PT3A and EGMA-PT4A was reflected by the distinctive increase in both T_g (from −3 to 50 °C) and gel content (from 76.7 to 92.2%). The related diffusion limitations slow down the reaction and reduce the final monomer conversion. This can be clearly seen by the decrease of the final acrylate conversions and the lower yield of acrylate homo-polymerization at higher degree of acrylate functionality.

The final thiol conversions significantly increased from 55% (EGMA-HP1A) to 77% (EGMA-PT4A), which is also attributed to the lower stoichiometric ratio of thiols with respect to acrylate functional groups (1:2 in EGMA-HP1A versus 1:5 in EGMA-PT4A). The results suggest that the rate of acrylate homo-polymerization slows down at higher conversions and higher degree of functionality whilst the step-growth reaction between thiol and acrylate groups becomes the dominating mechanism [65].

The higher crosslink density and lower number of –OH groups drastically slowed down the exchange kinetics of the transesterification (Fig. 5b). Whilst EGMA-HP1A required 530 s to relax 67% of its initial stress, the relaxation time was nearly one order of magnitude higher for EGMA-PT3A and EGMA-PT4A networks and amounted to 4825 s and

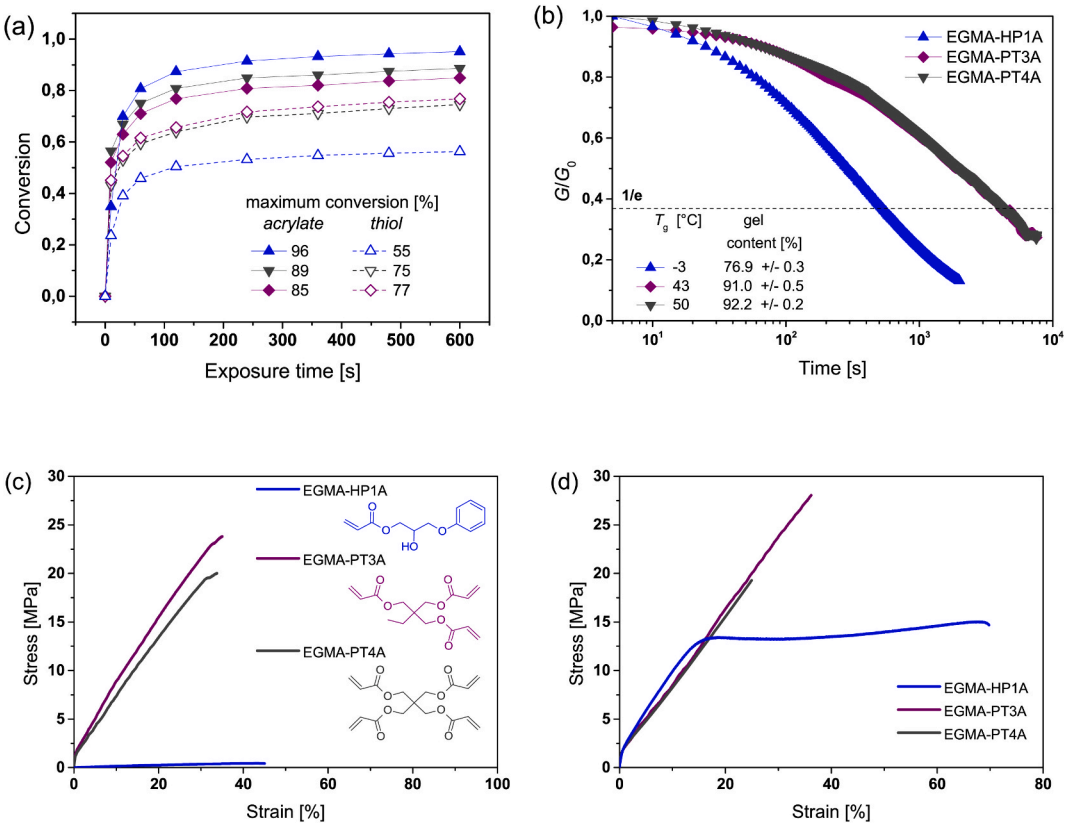

Fig. 5. (a) Cure kinetics and final monomer conversions of acrylate groups at 1635 cm^{-1} (full symbols) and thiol groups at 2570 cm^{-1} (open symbols) versus light exposure as obtained from FTIR experiments. While keeping the concentration of DG2A (25 mol%) constant, additional acrylate monomers with varying functionality have been used: EGMA-HP1A (blue up triangle), EGMA-PT3A (purple diamonds) and EGMA-PT4A (dark grey down triangles). The lines are a guide for the eye. (b) Normalized stress relaxation curves of thiol-acrylate vitrimers measured at 180 °C. The table provides the glass transition temperature (T_g) and gel content of the respective networks. Stress-strain curves of thiol-acrylate vitrimers containing acrylate monomers with varying functionality (c) prior to and (d) after a thermal annealing at 180 °C for 4 h.

4350 s, respectively.

With a T_g above room temperature (related DSC curves are provided in Fig. S3 in the supporting information), EGMA-PT3A and EGMA-PT4A were far stiffer than EGMA-HP1A, and comprised an ultimate elongation of 12% and 19% together with a tensile strength of 24 MPa and 20 MPa (Fig. 5c). The higher crosslink density and lower number of –OH groups also affected the tensile properties of the thermally annealed samples, which only slightly improved. For EGMA-PT3A, the tensile strength increased from 24 to 28 MPa whilst for EGMA-PT4A it remained nearly constant (Fig. 5d). From the results it can be concluded that the mechanical properties of thermally annealed thiol-acrylate vitrimers are affected by various parameters such as residual non-bonded monomers, crosslink density and inherent chemical structure of the monomers including the presence of ester and –OH groups, which are able to undergo thermo-activated exchange reactions.

In general, the low viscosity (330 mPa s obtained at a shear rate

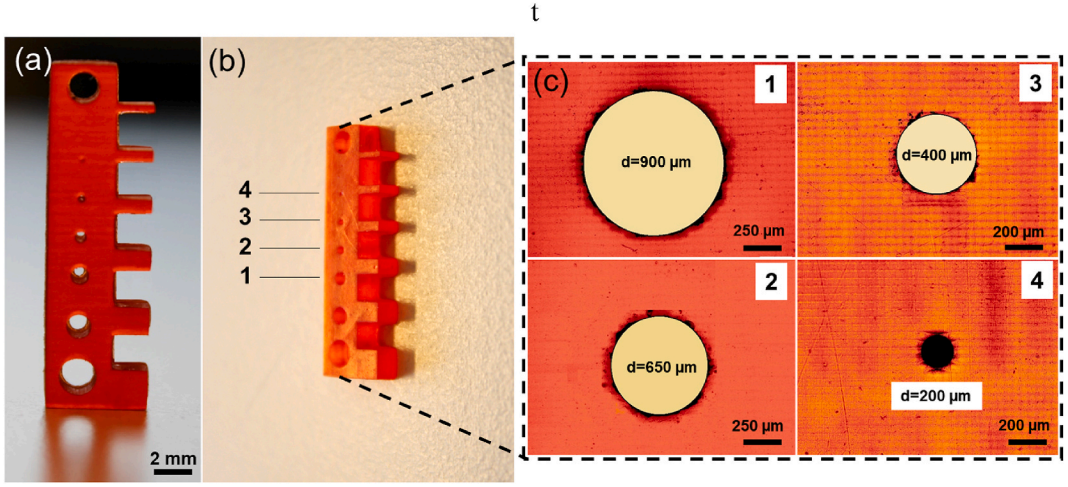

Fig. 6. Resolution of 3D objects obtained by DLP 3D-printing with EGMA-PT3A.

between 0.1 and 300 s^{-1}), the fast curing speed and adequate storage stability of EGMA-PT3A enabled the DLP 3D-printing of precise objects (Fig. 6a–b) with structure sizes of 200 μm (Fig. 6c). Further 3D objects obtained by DLP printing with EGMA-PT3A are provided in Fig. S4 in supporting information. Thus, for subsequent characterization of thermally induced characteristics and evaluation of healing performance, the test specimens were DLP 3D-printed with EGMA-PT3A.

3.3. Influence of thermal annealing on the properties of thiol-acrylate vitrimers

In previous work, we have demonstrated that a prolonged treatment at 180 °C does not only lead to topological rearrangements in thiol-acrylate vitrimers but also to the formation of additional crosslink sites and hydrogen bonding [39,62]. The stiffer network and the lower number of free –OH groups slows down the stress relaxation kinetics, whilst at the same time the mechanical properties (both tensile strength and elongation) are significantly improved. A similar behavior was also reported by Zhang and co-workers, who studied the properties of pure acrylate-based vitrimers prior to and after thermal annealing [66].

To characterize the impact of thermal annealing on the thiol-acrylate vitrimers under investigation, we selected two systems: EGMA-HP1A, as a soft network with a T_g well below room temperature, and EGMA-PT3A, a stiffer network with a T_g of 43 °C. For sample preparation, thin discs (d = 10 mm, h = 0.4 mm) were 3D printed and thermally annealed at 180 °C for 4 h under air. ATR FTIR spectra were taken prior to and after annealing and are provided in Fig. S5 and Fig. S6 in supporting information. In both systems, the characteristic thiol (2500-2600 cm^{-1}) and acrylate (1635 cm^{-1}) absorption bands slightly decreased indicating the formation of additional covalent bonds due to thermo-activated post-curing processes (e.g. additional formation of thioether links, C-C bond formation between two acrylate moieties or disulfide formation by oxidation of free thiol groups). In contrast, a strong depletion was observed for the broad absorption band related to the –OH groups (3200-3600 cm^{-1}) giving rise to distinctive hydrogen bonding. The thermo-activated change in crosslink density is also confirmed by the increase in the gel content, which is more pronounced in the softer EGMA-HP1A network (from 76.9 to 89.1%) compared to the stiffer EGMA-PT3A system (from 91.0 to 96.1%). This effect might be related to the higher amount of un-reacted thiols in the EGMA-HP1A network, which are prone to disulfide formation under oxidative conditions. Although disulfides are a prominent binding motif in the design of vitrimer networks [21,41,66–68], it is not expected that they play a major role in the stress relaxation kinetics of the thermally annealed thiol-acrylate vitrimers under investigation. As obtained from stress relaxation experiments, it is obvious that the additionally introduced crosslinks are not dynamic in nature as the stress relaxation kinetics of thermally annealed samples slows down (Fig. 7).

This effect is even more pronounced for EGMA-HP1A, which is in good agreement with the higher increase in gel content. The additional formation of permanent links leads to a lower network mobility, which is also confirmed by the increase of the T_g from −3 to 21 °C. The same trend was also observed for EGMA-PT3A. The lower mobility together with the reduced availability of free –OH groups (due to hydrogen bonding) slows down the exchange kinetics and the stress relaxation becomes less efficient. In particular for EGMA-HP1A, the time required to relax 67% of the initial stress increased from 530 to 1,810 s due to thermal annealing whilst for EGMA-PT3A it changed from 4,825 s to 10,900 s. It should be noted that although the values are shifted to longer times, the ranking of the networks does not change after the thermal annealing. Thus, stresses are still being relaxed much faster in EGMA-HP1A than in EGMA-PT3A.

3.4. DLP 3D-printing and thermally triggered healing of soft active devices

Among the studied thiol-acrylate vitrimers, EGMA-PT3A and EGMA-PT4A exhibited a T_g above room temperature. In particular, EGMA-PT3A was chosen for the fabrication of a soft active device since the network was characterized by a higher tensile strength. For the thermal actuation experiment, a spring actuator with 50 mm in length and 15 mm in diameter was fabricated by DLP 3D-printing (Fig. 8a). In the programming step, a weight, which was two times higher than the actuator, was fixed to the spring and the device was heated to 65 °C (Fig. 8b). Due to the softening of the actuator above its T_g (43 °C) with a corresponding reduction in the elastic modulus, the spring could be stretched to an elongation of around 70%.

Although the stretchability of EGMA-PT3A is limited as shown by tensile tests (ultimate elongation amounted to 36%), larger deformations were obtained due to the helical geometry of the 3D-printed actuator. By cooling down the actuator to 20 °C, the spring was able to lift the attached weight and retracted nearly to its original position in 60 s (Fig. 8b) as a result of the increase in elastic modulus below the T_g. This experiment was performed multiple times and a full recovery of the original helical shape was achieved (Fig. 8c and d).

In a subsequent experiment, the actuator was intentionally stretched to more than 80% of its initial length during the programming step, which led to a breakage of the spring (Fig. 9a). One of the unique features of vitrimers is their malleability and viscoelastic reflow above T_v, which can be exploited to thermally heal damages introduced into the 3D-printed test specimen. Although EGMA-PT3A exhibited a slow exchange rate due its higher crosslink density and low number of –OH groups in the network, the viscoelastic reflow was efficient enough to thermally heal the broken spring at 180 °C for 4 h (Fig. 9a). The thermally healed spring could be programmed again and was able to lift the same weight giving rise to the high healing efficiency of the network under investigation.

To quantify the healing efficiency, uniaxial tensile tests of DLP 3D-printed and thermally annealed test specimens were performed and

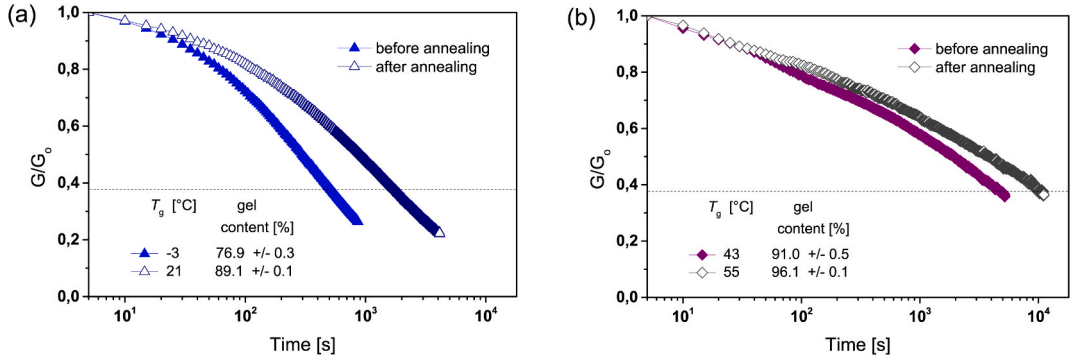

Fig. 7. Normalized stress relaxation curves of (a) EGMA-HP1A and (b) EGMA-PT3A vitrimers prior to and after thermal annealing at 180 °C for 4 h under air. The tables provide the glass transition temperature (T_g) and gel content of the respective networks.

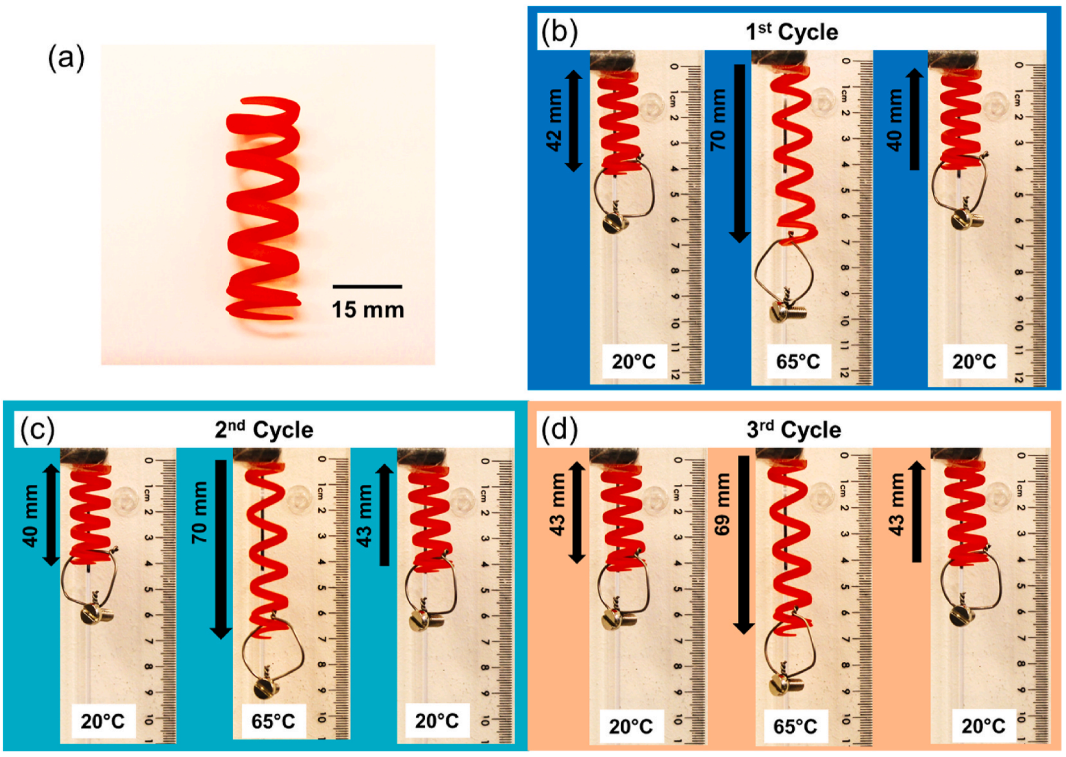

Fig. 8. (a) DLP 3D-printed spring actuator. (b) Attachment of a weight (2.9 g) on the actuator (1.5 g), which led to a deformation of the spring, when it was heated at 65 °C. The spring retracted back to its original shape by cooling the actuator to 20 °C and was able to lift the weight. Repeated movements of the spring by switching the temperature: (c) second actuation cycle (d) third actuation cycle showing a full recovery of the original shape of the spring.

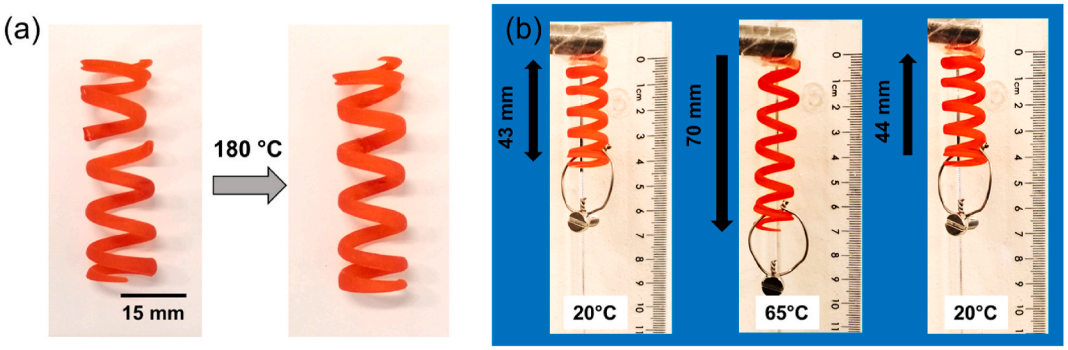

Fig. 9. (a) DLP 3D-printed spring actuator, which was thermally healed at 180 °C for 4 h. (b) Performance of the healed spring actuator during programming and recovery of permanent shape.

the ratio of the tensile strength prior to and after healing was determined. It should be noted that an appropriate aligning of the thin broken test bars was not possible. Thus, samples with a circular-shaped hole in the center were DLP 3D-printed and for the repair step, the circular-shaped counterpart was printed and fitted in the hole (Fig. 10a). The samples were then thermally annealed at 180 °C for 4 h and the tensile properties were compared to a defect-free control bar. The tensile properties clearly confirm the high healing efficiency as the original elongation could be fully recovered, whilst the tensile strength of the healed test specimen was even slightly higher compared to the control sample (Fig. 10b).

4. Conclusions

In this study, a library of thiols and acrylate monomers were comprehensively studied for their application in DLP printable thiol-acrylate vitrimers. In particular, by varying structure, functionality and the number of ester moieties of the monomers, clear structure-property relationships with the photo-reactivity, network adaptability and thermo-mechanical properties of DLP 3D-printed vitrimers were established. The results revealed that the presence of ester moieties accelerate both cure kinetics and stress relaxation rate of related thiol-acrylate vitrimers and facilitate a better mechanical performance of the dynamic network after a thermal annealing at 180 °C for 4 h. In contrast, increasing the functionality of the thiols or acrylate monomers slowed down the cure kinetics due to diffusion limitations of the mixed mode photopolymerization kinetics. Whilst the influence of the thiol functionality on the glass transition temperature (T_g) of the networks under investigation is negligible (−5 °C to −8 °C), the T_g significantly increased from −7 °C to 50 °C, by exchanging the mono-functional HP1A with the tetra-functional PT4A. Although the higher T_g networks were characterized by a slower stress relaxation rate, healing experiments revealed that the original properties of DLP 3D-printed test specimen can be fully recovered after thermally annealing EGMA-PT3A

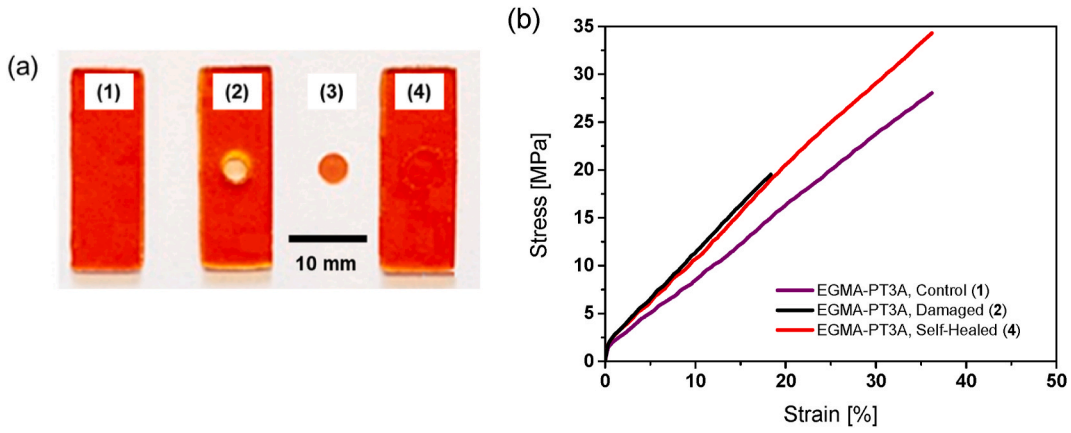

Fig. 10. (a) Photographs of DLP 3D-printed test specimen obtained from EGMA-PT3A: (1) defect-free control sample, (2) damaged sample with circular-shaped cavity in the center, (3) circular shaped counterpart for thermal healing and (4) healed test specimen after fitting the circular shaped counterpart in the hole and subsequent thermal treatment at 180 °C for 4 h. (b) Stress-strain curves of the control, damaged and thermally healed (180 °C for 4 h).

networks at 180 °C for 4 h. The good resolution of the 3D-printed parts (structure size of 400 μm could be successfully replicated) was exploited to fabricate soft actuators, which were repeatedly able to lift an object (2 times heavier than the actual weight of the actuator). By heating the actuator above its T_g (43 °C), the spring underwent an elongation of up to 70% and was able to recover its original shape by subsequent cooling of the sample below its T_g. The soft actuator also retained its function after breakage and subsequent thermal healing at 180 °C for 4 h.

CRediT authorship contribution statement

Usman Shaukat: Conceptualization, Methodology, Investigation, Writing – original draft, Visualization. **Elisabeth Rossegger:** Validation, Methodology, Supervision. **Sandra Schlögl:** Conceptualization, Writing – review & editing, Supervision, Funding acquisition.

Declaration of competing interest

The authors declare that they have no known competing financial interests or personal relationships that could have appeared to influence the work reported in this paper.

Acknowledgements

Part of the research work was performed with the "SMART" project. This project has received funding from the European Union's Horizon 2020 research and innovation programme under the Marie Sklodowska-Curie grant agreement No 860108. Part of the research work was performed also within the COMET-Module "Chemitecture" (project-no.: 21647048) at the Polymer Competence Center Leoben GmbH (PCCL, Austria) within the framework of the COMET-program of the Federal Ministry for Transport, Innovation and Technology and the Federal Ministry for Digital and Economic Affairs with contributions by the Institute of Chemistry of Polymeric Materials (Montanuniversitaet Leoben, Austria). The PCCL is funded by the Austrian Government and the State Governments of Styria, Upper and Lower Austria. In addition, the authors thank Florian Wanghofer (PCCL) for performing the DSC measurements.

Appendix A. Supplementary data

Supplementary data to this article can be found online at https://doi.org/10.1016/j.polymer.2021.124110.

References

[1] P.C. Hiemenz, T. Lodge, Polymer Chemistry, CRC Press, Boca Raton, [Florida], 2007.
[2] M. Rubinstein, R. Colby, Polymer Physics, OXFORD UNIVERSITY PRESS, 2003.
[3] P.J. Flory, Principles of Polymer Chemistry, first ed., Cornell Univ. Press, Ithaca, 1953.
[4] M. Hayashi, S. Matsushima, A. Noro, Y. Matsushita, Macromolecules 48 (2) (2015) 421–431.
[5] W. Alabiso, S. Schlögl, Polymers 12 (8) (2020) 1660.
[6] W. Denissen, J.M. Winne, F.E. Du Prez, Chem. Sci. 7 (1) (2016) 30–38.
[7] B. Krishnakumar, R.P. Sanka, W.H. Binder, V. Parthasarthy, S. Rana, N. Karak, Chem. Eng. J. 385 (2020), 123820.
[8] A. Demongeot, R. Groote, H. Goossens, T. Hoeks, F. Tournilhac, L. Leibler, Macromolecules 50 (16) (2017) 6117–6127.
[9] M. Capelot, D. Montarnal, F. Tournilhac, L. Leibler, J. Am. Chem. Soc. 134 (18) (2012) 7664–7667.
[10] Y.-X. Lu, F. Tournilhac, L. Leibler, Z. Guan, J. Am. Chem. Soc. 134 (20) (2012) 8424–8427.
[11] M. Röttger, T. Domenech, R. van der Weegen, A. Breuillac, R. Nicolaÿ, L. Leibler, Science (New York, N.Y.) 356 (6333) (2017) 62–65.
[12] M.O. Saed, A. Gablier, E.M. Terentejv, Adv. Funct. Mater. 30 (3) (2020), 1906458.
[13] O.R. Cromwell, J. Chung, Z. Guan, J. Am. Chem. Soc. 137 (20) (2015) 6492–6495.
[14] W. Denissen, G. Rivero, R. Nicolaÿ, L. Leibler, J.M. Winne, F.E. Du Prez, Adv. Funct. Mater. 25 (16) (2015) 2451–2457.
[15] W. Denissen, M. Droesbeke, R. Nicolaÿ, L. Leibler, J.M. Winne, F.E. Du Prez, Nat. Commun. 8 (2017), 14857.
[16] M. Guerre, C. Taplan, R. Nicolaÿ, J.M. Winne, F.E. Du Prez, J. Am. Chem. Soc. 140 (41) (2018) 13272–13284.
[17] T. Stukenbroeker, W. Wang, J.M. Winne, F.E. Du Prez, R. Nicolaÿ, L. Leibler, Polym. Chem. 8 (43) (2017) 6590–6593.
[18] A. Ruiz de Luzuriaga, R. Martin, N. Markaide, A. Rekondo, G. Cabañero, J. Rodríguez, et al., Mater. Horiz. 3 (3) (2016) 241–247.
[19] Z.Q. Lei, H.P. Xiang, Y.J. Yuan, M.Z. Rong, M.Q. Zhang, Chem. Mater. 26 (6) (2014) 2038–2046.
[20] M. Chen, L. Zhou, Y. Wu, X. Zhao, Y. Zhang, ACS Macro Lett. 8 (3) (2019) 255–260.
[21] J. Canadell, H. Goossens, B. Klumperman, Macromolecules 44 (8) (2011) 2536–2541.
[22] L. Lu, J. Pan, G. Li, J. Mater. Chem. 5 (40) (2017) 21505–21513.
[23] K. Yu, P. Taynton, W. Zhang, M.L. Dunn, H.J. Qi, RSC Adv. 4 (20) (2014) 10108–10117.
[24] J.P. Brutman, P.A. Delgado, M.A. Hillmyer, ACS Macro Lett. 3 (7) (2014) 607–610.
[25] S. Kaiser, S. Wurzer, G. Pilz, W. Kern, S. Schlögl, Soft Matter 15 (30) (2019) 6062–6072.
[26] S. Kaiser, J. Jandl, P. Novak, S. Schlögl, Soft Matter 16 (37) (2020) 8577–8590.
[27] P. Yan, W. Zhao, X. Fu, Z. Liu, W. Kong, C. Zhou, et al., RSC Adv. 7 (43) (2017) 26858–26866.
[28] W. Denissen, I de Baere, W. van Paepegem, L. Leibler, J. Winne, F.E. Du Prez, Macromolecules 51 (5) (2018) 2054–2064.
[29] J. Han, T. Liu, C. Hao, S. Zhang, B. Guo, J. Zhang, Macromolecules 51 (17) (2018) 6789–6799.
[30] F.I. Altuna, C.E. Hoppe, R.J. Williams, Eur. Polym. J. 113 (2019) 297–304.
[31] M. Hayashi, R. Yano, A. Takasu, Polym. Chem. 10 (16) (2019) 2047–2056.
[32] S. Zhao, M.M. Abu-Omar, Macromolecules 52 (10) (2019) 3646–3654.
[33] Z. Pei, Y. Yang, Q. Chen, Y. Wei, Y. Ji, Adv. Mater. 28 (1) (2016) 156–160.
[34] M. Capelot, M.M. Unterlass, F. Tournilhac, L. Leibler, ACS Macro Lett. 1 (7) (2012) 789–792.
[35] D. Montarnal, M. Capelot, F. Tournilhac, L. Leibler, Science (New York, N.Y.) 334 (6058) (2011) 965–968.

[36] G. Mashouf Roudsari, A.K. Mohanty, M. Misra, ACS Sustain. Chem. Eng. 5 (11) (2017) 9528–9541.
[37] D.K. Patel, A.H. Sakhaei, M. Layani, B. Zhang, Q. Ge, S. Magdassi, Adv. Mater. 29 (15) (2017), 1606000.
[38] Z. Ji, X. Zhang, C. Yan, X. Jia, Y. Xia, X. Wang, et al., Macromol. Rapid Commun. 40 (8) (2019), e1800873.
[39] E. Rossegger, R. Höller, D. Reisinger, J. Strasser, M. Fleisch, T. Griesser, et al., Polym. Chem. 12 (5) (2021) 639–644.
[40] G.B. Lyon, L.M. Cox, J.T. Goodrich, A.D. Baranek, Y. Ding, C.N. Bowman, Macromolecules 49 (23) (2016) 8905–8913.
[41] K. Yu, an Xin, H. Du, Y. Li, Q. Wang, NPG Asia Mater. 11 (1) (2019).
[42] X. Feng, G. Li, ACS Appl. Mater. Interfaces 12 (51) (2020) 57486–57496.
[43] B.J. Blaiszik, S. Kramer, S.C. Olugebefola, J.S. Moore, N.R. Sottos, S.R. White, Annu. Rev. Mater. Res. 40 (1) (2010) 179–211.
[44] S.J. Benight, C. Wang, J.B. Tok, Z. Bao, Prog. Polym. Sci. 38 (12) (2013) 1961–1977.
[45] M. Zarek, M. Layani, I. Cooperstein, E. Sachyani, D. Cohn, S. Magdassi, Adv. Mater. 28 (22) (2016) 4449–4454.
[46] R.A. Bilodeau, R.K. Kramer, Front. Robot. AI 4 (2017) 48.
[47] D. Rus, M.T. Tolley, Nature 521 (7553) (2015) 467–475.
[48] X. Zheng, W. Smith, J. Jackson, B. Moran, H. Cui, Da Chen, et al., Nat. Mater. 15 (10) (2016) 1100–1106.
[49] X. Zheng, H. Lee, T.H. Weisgraber, M. Shusteff, J. DeOtte, E.B. Duoss, et al., Science 344 (6190) (2014) 1373–1377.
[50] E. Rossegger, R. Höller, D. Reisinger, M. Fleisch, J. Strasser, V. Wieser, et al., Polymer 221 (2021), 123631.
[51] K. Moazzen, E. Rossegger, W. Alabiso, U. Shaukat, S. Schlögl, Macromol. Chem. Phys. (2021), 2100072.
[52] B.H. Northrop, R.N. Coffey, J. Am. Chem. Soc. 134 (33) (2012) 13804–13817.
[53] M.J. Kade, D.J. Burke, C.J. Hawker, J. Polym. Sci. A Polym. Chem. 48 (4) (2010) 743–750.
[54] C.E. Hoyle, C.N. Bowman, Angew. Chem. 49 (9) (2010) 1540–1573.
[55] A. Dondoni, Angew. Chem. 47 (47) (2008) 8995–8997.
[56] C.E. Hoyle, A.B. Lowe, C.N. Bowman, Chem. Soc. Rev. 39 (4) (2010) 1355–1387.
[57] C.E. Hoyle, T.Y. Lee, T. Roper, J. Polym. Sci. A Polym. Chem. 42 (21) (2004) 5301–5338.
[58] M. Sahin, S. Ayalur-Karunakaran, J. Manhart, M. Wolfahrt, W. Kern, S. Schlögl, Adv. Eng. Mater. 19 (4) (2017), 1600620.
[59] O. van den Berg, L.-T.T. Nguyen, R.F.A. Teixeira, F. Goethals, C. Özdilek, S. Berghmans, et al., Macromolecules 47 (4) (2014) 1292–1300.
[60] S.V. Radl, C. Schipfer, S. Kaiser, A. Moser, B. Kaynak, W. Kern, et al., Polym. Chem. 8 (9) (2017) 1562–1572.
[61] M. Hayashi, R. Yano, Macromolecules 53 (1) (2020) 182–189.
[62] S. Wang, N. Teng, J. Dai, J. Liu, L. Cao, W. Zhao, et al., Polymer 210 (2020), 123004.
[63] E. Andrzejewska, Prog. Polym. Sci. 26 (4) (2001) 605–665.
[64] C. Li, M. Johansson, P. Buijsen, G. Dijkstra, R.J. Sablong, C.E. Koning, Prog. Org. Coating 151 (2021), 106073.
[65] A.F. Senyurt, H. Wei, C.E. Hoyle, S.G. Piland, T.E. Gould, Macromolecules 40 (14) (2007) 4901–4909.
[66] B. Zhang, K. Kowsari, A. Serjouei, M.L. Dunn, Q. Ge, Nat. Commun. 9 (1) (2018) 1831.
[67] X. Li, R. Yu, Y. He, Y. Zhang, X. Yang, X. Zhao, et al., ACS Macro Lett. 8 (11) (2019) 1511–1516.
[68] S. Nevejans, N. Ballard, J.I. Miranda, B. Reck, J.M. Asua, Phys. Chem. Chem. Phys. PCCP 18 (39) (2016) 27577–27583.